J. Phys. B: At. Mol. Opt. Phys. **30** (1997) 729–747. Printed in the UK PII: S0953-4075(97)73282-6

Electron-impact ionization of neon ions ($q = 4$–8)

M Duponchelle†, M Khouilid‡, E M Oualim§, H Zhang† and P Defrance†

† Université Catholique de Louvain, Département de Physique, Chemin du Cyclotron 2, B-1348 Louvain-la-Neuve, Belgium

‡ Université Chouaib Doukkali, Faculté des Sciences, Km1, Route Ben Maachou, BP 20, El Jadida, Morocco

Received 2 April 1996, in final form 17 September 1996

Abstract. Absolute cross section measurements for electron-impact single ionization of Ne^{q+} ($q = 4$–8) ions and for double ionization of Ne^{5+} and Ne^{6+} are reported. The animated crossed-beams method has been applied. The measurements cover the energy range from threshold to several keV. The Ne^{4+} and Ne^{6+} ion beams are found to contain an important population of ions formed in metastable states. For single ionization, results are in overall good agreement with direct ionization theoretical predictions, when available. Excitation–autoionization is observed in the ionization threshold region for Ne^{4+} and in the K–L transition energy region for Ne^{6+} and Ne^{7+}. Double ionization of Ne^{5+} and Ne^{6+} is found to be dominated by K-shell ionization followed by autoionization.

1. Introduction

Neon is frequently introduced in tokamaks as a diagnostic element for probing fusion plasmas. For this reason, a good knowledge of related spectroscopic and collisional atomic data is needed in order to interpret the observation of various plasma parameters (Janev 1993). Among the processes playing a role in this field, electron-impact ionization of atoms or ions is a fundamental one, because it governs the ion charge state distribution evolution in the plasma so that the corresponding ionization cross sections are required for plasma modelling. The status of the knowledge of the electron-impact ionization process has been analysed in detail (Defrance *et al* 1995) for ions of thermonuclear interest.

For single ionization (SI), various applications of the Coulomb–Born approximation have produced theoretical results for five neon ions (Ne^{q+}, $q = 1, 2, 6$–8) and the R-matrix theory has been applied to Ne^{6+} only (Laghdas *et al* 1995). In addition, the K-shell ionization–autoionization (IA) process was also included in this calculation. This is the one and only result for double ionization (DI), as there are no theoretical results available for direct double ionization (DDI).

High-energy (2.7–10 keV) cross sections for electron-impact single ionization of neon ions ($q = 1$–9) have been first deduced from the analysis of the charge state distribution evolution for ions extracted from an electron beam ion source (EBIS, Donets and Ovzyiannikov 1981). Absolute crossed-beams results have been obtained for charge states 1 (Man *et al* 1987, for example), 2 (Matsumuto *et al* 1990), 3 (Gregory *et al* 1983) and 7 (Defrance *et al* 1990), only.

§ Present address: Université Chouaib Doukkali, Faculté des Sciences et Techniques, BP 577, route de Casablanca, Settat, Morocco.

0953-4075/97/030729+19$19.50

In this paper, absolute cross sections are reported for electron-impact ionization of multiply-charged neon ions: first single ionization data for $q = 4$, 5, 6 and 8, new data for $q = 7$ and first double ionization data for $q = 5$ and 6.

2. Apparatus

In the experiments, the animated crossed-beams method (Defrance *et al* 1981) has been employed. The present apparatus is described in detail elsewhere (Duponchelle *et al* 1995). It has been specially designed to study electron-impact single and multiple ionization of multiply charged ions (X^{q+}) up to $q = 20$ in an electron energy range from 20–6000 eV.

The device is shown schematically in figure 1. The ion beam is extracted from an electron cyclotron resonance (ECR) ion source (1), accelerated by a voltage of 10 kV, mass-analysed (2), deflected and focused to the collision region by a vertical lens (3) and by two cylindrical deflectors (4), (5). The beam is collimated to a cross section of 2×4 mm^2 before crossing the electron beam (6). The magnetic mass analyser (7) separates the product ions $X^{(q+m)+}$ from the primary ions $X^{(q+)}$. The product ions are transmitted via a spherical deflector (10) to the channeltron detector (11) while the primary ions are collected by a Faraday cup (8) or (9), depending on the initial and final ion charges.

The high-voltage electron gun is shown schematically in the inset in figure 1. The ribbon electron beam is produced in a Pierce cathode–anode configuration by an impregnated

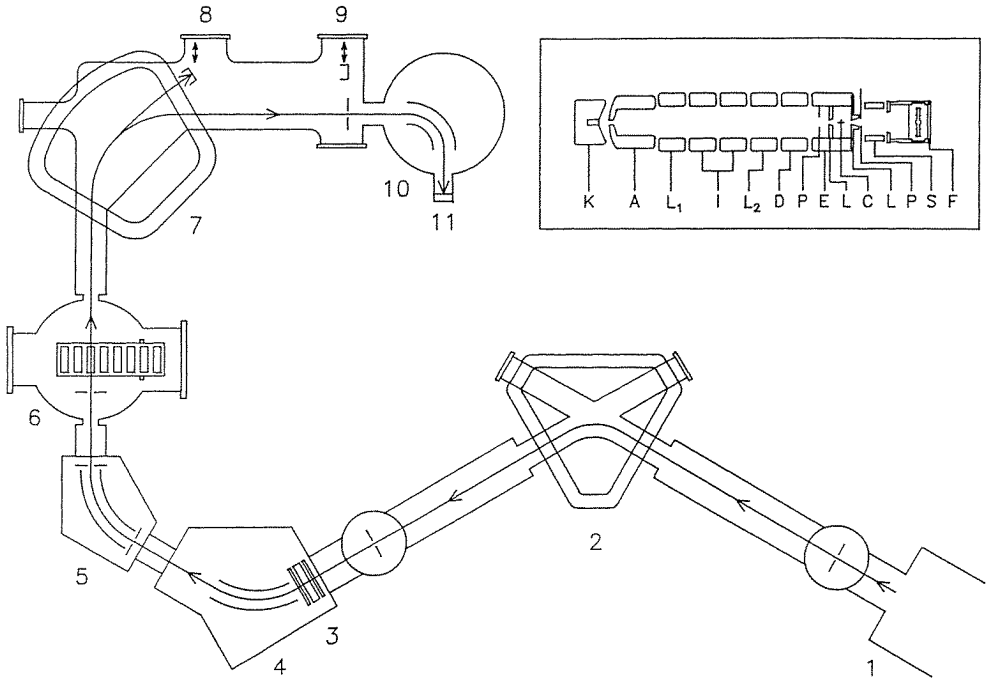

Figure 1. Schematic representation of the apparatus: 1, ECR ion source; 2, magnetic mass selector; 3, electrostatic lens; 4, 5, cylindrical deflectors; 6, collision chamber; 7, magnetic analyser; 8, 9, Faraday cups; 10, spherical deflector; 11, channeltron detector. The inset shows a schematic plan of the electron gun: K, cathode; A, anode; L_1–L_2–I, focusing electrodes; D, deflectors; P-S, suppressors; E, final electrodes; L, slits; C, collision region; F, Faraday cup.

cathode (K). The anode (A) forms a pair of parallel plates which is used as the first element of a pair of two electrostatic plane asymmetric lenses. These are designed to progressively accelerate the electrons to their final energy. The pairs of electrodes (L_1) and (L_2) are the central parts of the first and of the second lens, respectively. They are separated by the intermediate electrodes (I). Electrodes (D) act as a beam deflector and plates (E) define a zero equipotential region where the beams are crossing at right angles (C). The kinetic energy of the electron beam is controlled by the voltage difference between the cathode (K) and the electrodes (E). On both sides of the interaction region, slits (L) collimate the beam and plates (P) play the role of suppressors. A voltage can be applied to these plates in order to establish a potential barrier or a potential well to check the influence of residual gas ions trapped in the electron beam. The electron beam is collected in a Faraday cup (F). Suppressing electrodes (S) provide total beam collection and prevent secondary electrons from interacting with the ion beam. As required by the animated beam method, the electron beam is swept mechanically across the ion beam in a see-saw motion. The electron gun displacement is produced by means of a step by step motor acting on a rod. An optical encoder records the gun position with a precision of 2 μm.

In this kind of experiment, the count rate (N) is related to the cross section (σ) by the general relation

$$N = L\sigma \tag{1}$$

where L is the luminosity. In the present application of the animated beam method, the ionization cross section is related to the measured quantities in the following way (Duponchelle *et al* 1995):

$$\sigma = \frac{H}{n}\frac{qe^2 v_e v_i}{\sqrt{v_e^2 + v_i^2}}\sum_{j=1}^{n}\frac{k(j)}{\Delta t(j) i_e(j) i_i(j)} \tag{2}$$

where $k(j)$ is the number of events produced at position j of the sweeping motion for one passage of the electrons across the ion beam, $\Delta t(j)$ is the time spent at this position, v_e and v_i, e and qe, $i_e(j)$ and $i_i(j)$, are the velocities, charges and currents of the electrons and of the ions, respectively. H is the total vertical displacement of the electron beam and n is the number of steps.

3. Measurements

Four recordings take place simultaneously. The electron and ion currents collected in Faraday cups are frequency converted and recorded according to the electron beam position in a multichannel analyser triggered by the signals showing the position of the encoder. Similar recordings are performed for the amplified detector pulses and for the pulses produced by the internal clock of the computer. The number of events is divided by the time spent at each position and by the corresponding electron and ion currents so that irregularities due to mechanical perturbations do not affect the precision of the cross section measurements.

The detector efficiency has been estimated to be 100% from the pulse height spectrum observation and the total transmission of ions from the collision to the detector has been established. The electron-impact ionization signal is proportional to the ion and electron currents. The background consists of two distinct contributions. The first one is independent of the particle currents and is caused by the intrinsic background of the detector and by x-rays emitted by the ECR ion source. The second one, which is proportional to the ion current,

is due to interactions of primary ions with slits and with residual gas molecules. Reactions producing ions of the same charge and energy as the true signal are charge exchange and stripping. In addition, slow secondary ions may be formed by electron impact on residual gas or at the collector. They can be avoided by suitable polarization of this collector (F) and of the suppressing electrodes (P) and (S). The background from the residual gas is deduced from the flat areas of the spectrum after substraction of the intrinsic background of the detector.

In the case of single ionization both contributions, intrinsic background of the detector and background on residual gas, are present. In the case of double ionization, only the intrinsic background of the detector is present.

It is not possible to separate ions having the same charge-to-mass ratio. This situation holds for the Ne^{5+} primary ion beam which is seen to contain C^{3+} and O^{4+} ions, so that the true primary ion current is overestimated in the experiment. Absolute cross section measurement requires making use of the neon isotope Ne^{22} (natural abundance 8.8%) or determining the impurity ion population. For this purpose, the following procedure can be adopted. By adjusting the analysing magnetic field, it is possible to collect separately the low-intensity Ne^{4+}, C^{2+} and O^{3+} beams produced by the corresponding primary ions capturing an electron from the residual gas. The measured currents are proportional to the Ne^{5+}, C^{3+} and O^{4+} population and to the respective capture cross section. The capture cross sections are well known (Bliman *et al* 1983), so that the comparison of measured

Table 1. Typical working conditions.

Parameter	Typical value	Error (%) Systematic	Error (%) Statistical
Kinematic factor		0.5	—
Velocity (u, mm s^{-1})	0.48	0.1	—
Electron current (I_e)	7–17 mA	0.5	1.0
Ion current (I_i)			
Ne^{4+}	330 nA	0.5	1.0
Ne^{5+} (mass = 22)	30 nA	0.5	1.0
Ne^{5+} (mass = 20)	630 nA	0.5	1.0
Ne^{6+}	300 nA	0.5	1.0
Ne^{7+}	225 nA	0.5	1.0
Ne^{8+}	50 nA	0.5	1.0
Counts (K); luminosity (L, 10^{19} Hz cm^{-2})			
Ne^{4+}(SI)	11 000/6.9	1.0	2.5
Ne^{5+}(SI)	560/0.9	1.0	2.8
Ne^{5+}(DI)	500/87	1.0	2.7
Ne^{6+}(SI)	9500/9.9	1.0	2.7
Ne^{6+}(DI)	150/29	1.0	3.9
Ne^{7+}(SI)	950/26	1.0	2.8
Ne^{8+}(SI)	180/32	1.0	8.8
Cross section (σ, 10^{-19} cm^2)			
Ne^{4+}(SI)	40	2.6	4.5
Ne^{5+}(SI)	1.78	2.6	4.8
Ne^{5+}(DI)	0.26	2.6	4.7
Ne^{6+}(SI)	7.3	2.6	4.7
Ne^{6+}(DI)	0.23	2.6	5.9
Ne^{7+}(SI)	0.30	2.6	4.8
Ne^{8+}(SI)	0.25	2.6	10.8

currents with the primary ion beam intensity allows the relative impurity ion populations to be determined. Subsequently, the true Ne^{5+} current intensity is estimated with a satisfactory precision.

As the DI signal is very low for Ne^{5+}, the measurements were performed by using a high intensity Ne^{20} ion beam, but with clean source conditions. The cleanliness of the source affects the presence of impurities such as carbon and oxygen. It is therefore assumed that the cleanliness may also affect the metastable population. The impurity ion population was found to never exceed 1%, a figure which was taken into account in the cross section evaluation. The SI measurements were performed by using a Ne^{22} ion beam.

The electron energy is corrected for contact potential (-0.5 eV) and the kinetic energy of ions is taken into account to obtain the absolute collision energy (Duponchelle *et al* 1995). The uncertainty on this energy is ± 0.5 eV. Table 1 gives typical working conditions for the reactions under investigation here.

4. Results and discussion

Results are listed in tables 2–6 for SI of $Ne^{q+}(q = 4$–$8)$ and in tables 7 and 8 for DI of Ne^{5+} and Ne^{6+}. The energy levels relevant for the present discussion are given in figure 2. Ground-state ionization thresholds and singly excited states energies are extracted from the tables of Bashkin and Stoner (1975). Autoionizing states energies are experimental ones for Ne^{7+} (Schumann *et al* 1977) and calculated ones for the other cases (Clementi and Roetti (1974) for $Ne^{4,5+}$ and Chen and Crasemann (1987) for Ne^{6+}).

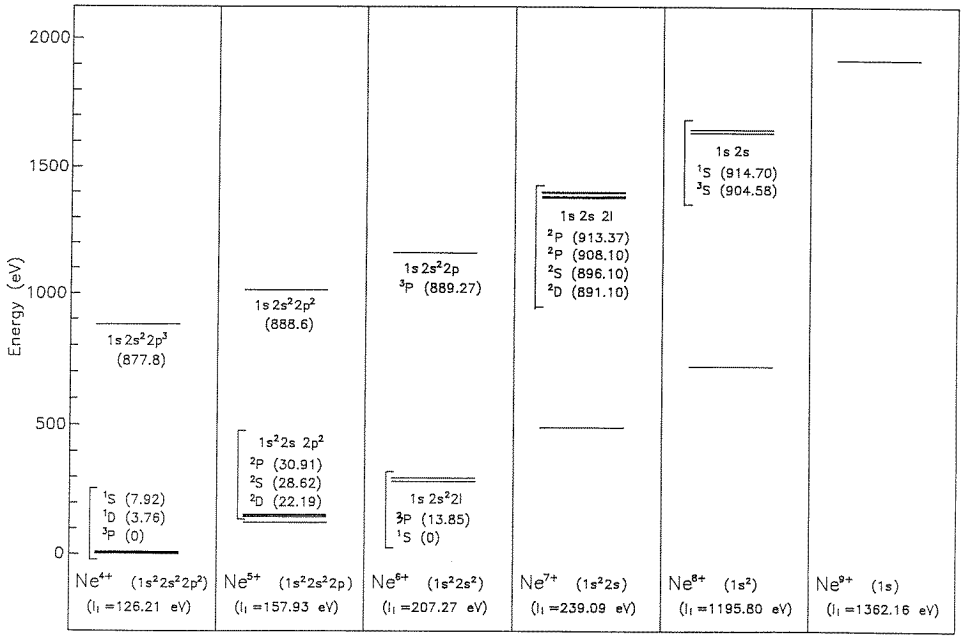

Figure 2. Ionization potentials (I_1) for ground states ions and energy levels for Ne^{q+} ions ($q = 4$–9). The energy levels are labelled by their configuration and state. The corresponding energies (eV) above the ground state are given in parentheses.

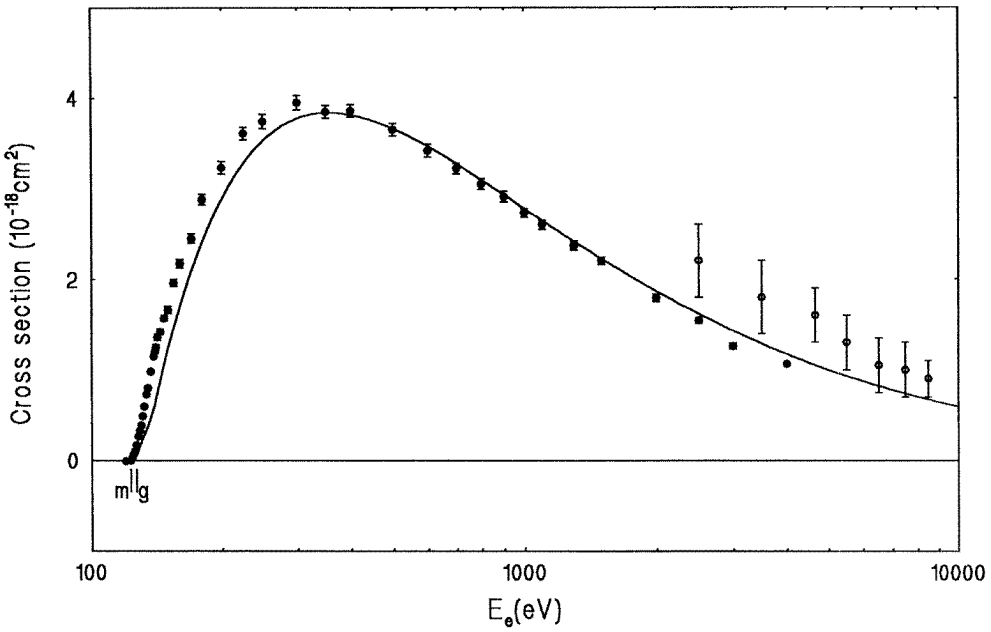

Figure 3. Absolute cross sections versus energy for electron-impact single ionization of Ne^{4+}. Full circles (●) are the present experimental results, the error bars are of one standard deviation statistical uncertainty. Two bars indicate the ionization thresholds for the ground state (g) and for the metastable state (m). The results of Donets and Ovsyannikov (1981) are also shown (○). The full curve is the semi-empirical Lotz formula for a mixing of ground and metastable states.

Results are also shown in figures 3–9. Error bars represent one standard deviation of the counting statistics, only. For single ionization, the experimental data of Donets and Ovzyannikov (1981) are also shown. They are some 30% higher than the present results for ion charges 4–6 but they are in fair agreement for charges 7 and 8. The discrepancy is probably due to the procedure adopted for the cross section estimation from the charge state spectra extracted from the EBIS source.

A zero cross section—within the statistical uncertainty—below the ground-state threshold indicates a negligible metastable excited-state population in the ion beam. For Ne^{4+} an important signal (see the next paragraph) is observed below the ground-state ionization threshold, indicating the presence of metastable states. For Ne^{6+}, two separate measurements have been performed. In the first one, particularly clean source conditions were obtained, so that no metastable population could be observed. In the second one, metastable states played an evident role. Data with a metastable contribution are noted by (m) in table 4. In contrast, no metastable population contribution was observed for Ne^{8+}.

4.1. Single ionization of Ne^{4+}

For Ne^{4+}, the threshold is clearly observed (figure 3) around 123 eV, which is 4 eV below the ground-state ionization threshold. The ground-state configuration of the carbon-like Ne^{4+} ion ($1s^2 2s^2 2p^2$) is formed by three states, the ^3P (ground state) and the ^1D and ^1S (excited states), which are 3.8 and 7.9 eV above the ground state, respectively. It is clear that the ion beam contains an important ^1D population, but no ^1S population. The metastable population (α) can be determined by fitting the low-energy experimental data, assuming a

Table 2. Total cross section for single ionization of Ne^{4+} by electron impact.

E_e (eV)	σ (10^{-18} cm^2)	$\Delta\sigma$ (10^{-18} cm^2)
122	−0.0019	0.0027
125	0.0005	0.001
127	0.07	0.01
129	0.17	0.01
130	0.27	0.01
131	0.33	0.01
132	0.39	0.01
133	0.49	0.01
134	0.60	0.01
136	0.73	0.02
137	0.80	0.02
139	0.98	0.02
141	1.15	0.02
142	1.32	0.03
146	1.42	0.03
149	1.57	0.03
152	1.66	0.04
157	1.96	0.04
162	2.17	0.05
172	2.45	0.05
182	2.88	0.06
202	3.23	0.07
227	3.61	0.07
252	3.74	0.08
302	3.95	0.08
352	3.85	0.07
402	3.86	0.07
502	3.65	0.07
602	3.42	0.07
702	3.22	0.06
802	3.05	0.06
902	2.91	0.06
1002	2.73	0.05
1102	2.6	0.05
1302	2.37	0.05
1502	2.20	0.04
2002	1.79	0.04
2502	1.54	0.03
3002	1.26	0.03
4002	1.06	0.02

similar energy dependence for both states close to the threshold. The Lotz formula, which gives the linear energy (E) dependence in the threshold energy region, was employed in the present case to determine the ground and metastable populations. The apparent cross section ($\sigma_a(E)$), was given by Lotz (1968):

$$\sigma_a(E) = \sigma_m(E) + (1 - \alpha)\sigma_g(E) \tag{3}$$

where $\sigma_g(E)$ and $\sigma_m(E)$ are the ground and metastable cross sections, respectively. The population of the metastable state is found to be 0.368, a figure which is very close to the statistical weight of this state (0.357).

Table 3. Total cross section for single ionization of Ne^{5+} by electron impact.

E_e (eV)	σ (10^{-18} cm^2)	$\Delta\sigma$ (10^{-18} cm^2)
141	−0.007	0.004
151	−0.028	0.1
157	0.027	0.084
159	0.0053	0.0023
161	0.015	0.03
171	0.32	0.03
181	0.59	0.06
201	0.99	0.05
226	1.31	0.06
251	1.6	0.06
271	1.76	0.06
301	2.02	0.07
351	2.12	0.07
401	2.14	0.08
501	2.08	0.07
601	1.87	0.05
701	1.78	0.05
801	1.61	0.05
901	1.53	0.05
1001	1.49	0.05
1201	1.32	0.05
1501	1.24	0.04
2001	1.00	0.03
3001	1.72	0.03
4001	0.58	0.03

No theoretical results can be compared to the present results. The scaling of the O^{2+} experimental data (Gregory *et al* 1985), as recommended by Lennon *et al* (1988), predicts a cross section which is about 10% lower than the present data around the maximum. The semi-empirical Lotz formula (1968) is applied with inclusion of the 2s and the 2p contributions for both the ground state and the metastable ^{1}D state and by taking into account their respective population. According to the simplicity of the Lotz formula, the result of this cross section prediction is surprisingly satisfactory. However, some of the features observed in the low-energy region cannot be explained by direct ionization processes. In particular, the change of slope observed at 140 eV seems to indicate the presence of indirect processes which are probably associated with the promotion of an electron from the 2s shell to higher levels. It is not possible to tell whether we can attribute this effect to the presence of metastable states or not.

4.2. Single ionization of Ne^{5+}

The single-ionization cross section is presented in figure 4 for Ne^{5+} together with the experimental data of Donets and Ovzyannikov (1981). Again, no theoretical or crossed-beams experimental results can be compared to the present ones which are in good agreement with the Lotz formula prediction. Indirect ionization mechanisms are not observed, in particular, in the K–L excitation energy region. They are probably too weak to be detected, as indicated by the very small K-shell ionization cross section which is found to be almost two orders of magnitude lower than the single one. K-shell ionization is nearly totally

Table 4. Total cross section for single ionization of Ne^{6+} by electron impact.

E_e (eV)	σ (10^{-19} cm^2)	$\Delta\sigma$ (10^{-19} cm^2)
151	0.27	0.41
176	−0.004	0.003
194 (m)	0.096	0.10
195 (m)	0.12	0.17
196 (m)	0.30	0.22
201	−0.056	0.07
201 (m)	0.34	0.18
206 (m)	0.67	0.19
211	0.47	0.10
216 (m)	1.15	0.20
226	1.22	0.19
251	2.66	0.24
276	4.19	0.27
301	4.51	0.23
326	5.91	0.39
351	6.10	0.28
376	6.79	0.27
401	6.77	0.27
401 (m)	7.17	0.22
426	6.91	0.22
451	7.22	0.26
476	7.19	0.27
501	7.28	0.21
501 (m)	7.43	0.20
551	7.26	0.22
601	7.14	0.13
651	7.13	0.19
701	6.78	0.18
751	6.75	0.14
801	6.62	0.23
851	6.81	0.17
901	6.80	0.14
951	6.86	0.18
1001	6.46	0.18
1201	6.12	0.17
1501	5.53	0.15
2001	4.51	0.12
2501	3.86	0.11
3001	3.42	0.10
4001	2.94	0.08
5001	2.32	0.10

followed by autoionization so that this indirect process contributes to double ionization only (see section 4.6 below).

4.3. Single ionization of Ne^{6+}

The Ne^{6+} metastable ($1s^2 2s 2p\ ^3P_1$) state lies 13.85 eV above the ground state and its lifetime was estimated as 240 μs by Cheng *et al* (1979). The low-energy results are presented in figure 5(*a*). The results of the first set of measurements below the ground-state ionization threshold show that the metastable fraction is negligible, although the time of flight of ions

Table 5. Total cross section for single ionization of Ne^{7+} by electron impact.

E_e (eV)	σ (10^{-19} cm^2)	$\Delta\sigma$ (10^{-19} cm^2)
221	−0.007	0.001
226	−0.0097	0.0022
231	−0.002	0.02
236	0.013	0.001
239	−0.002	0.001
241	0.06	0.048
251	0.29	0.12
261	0.65	0.11
271	0.81	0.11
281	1.11	0.11
301	1.42	0.12
321	1.61	0.08
351	2.09	0.17
401	2.50	0.17
451	2.63	0.14
501	2.77	0.08
601	2.87	0.10
701	2.84	0.10
751	2.86	0.09
801	2.83	0.06
841	2.76	0.08
881	2.76	0.08
891	2.82	0.09
896	2.83	0.10
901	2.90	0.09
906	3.02	0.07
911	3.11	0.09
916	3.16	0.11
921	3.21	0.10
926	3.17	0.08
931	3.18	0.10
951	3.17	0.11
1001	3.00	0.08
1051	3.05	0.08
1101	2.92	0.07
1151	2.94	0.08
1201	2.92	0.08
1301	2.82	0.08
1401	2.72	0.09
1601	2.63	0.09
1801	2.44	0.06
2001	2.28	0.07
2251	2.03	0.07
2501	1.92	0.07
3001	1.68	0.05
4001	1.42	0.06
5001	1.16	0.13

from the source to the collision region is only 6 μs. Moreover, the experimental data available for other members of the beryllium-like sequence (B^+, C^{2+}, N^{3+} and O^{4+}, Falk *et al* 1983) showed a high metastable ion population (50–90%) for all of these ions. In the second set of the present data, a large signal was observed below the ground-state ionization

Table 6. Total cross section for single ionization of Ne^{8+} by electron impact.

E_e (eV)	σ (10^{-20} cm^2)	$\Delta\sigma$ (10^{-20} cm^2)
901	−0.15	0.15
1051	0.29	0.25
1191	0.33	0.18
1401	0.77	0.23
1601	1.41	0.21
1801	1.56	0.21
2001	1.78	0.21
2251	1.96	0.16
2501	2.24	0.21
3001	2.51	0.20
3501	2.26	0.16
4001	2.54	0.20
4501	2.46	0.28
5001	2.34	0.24

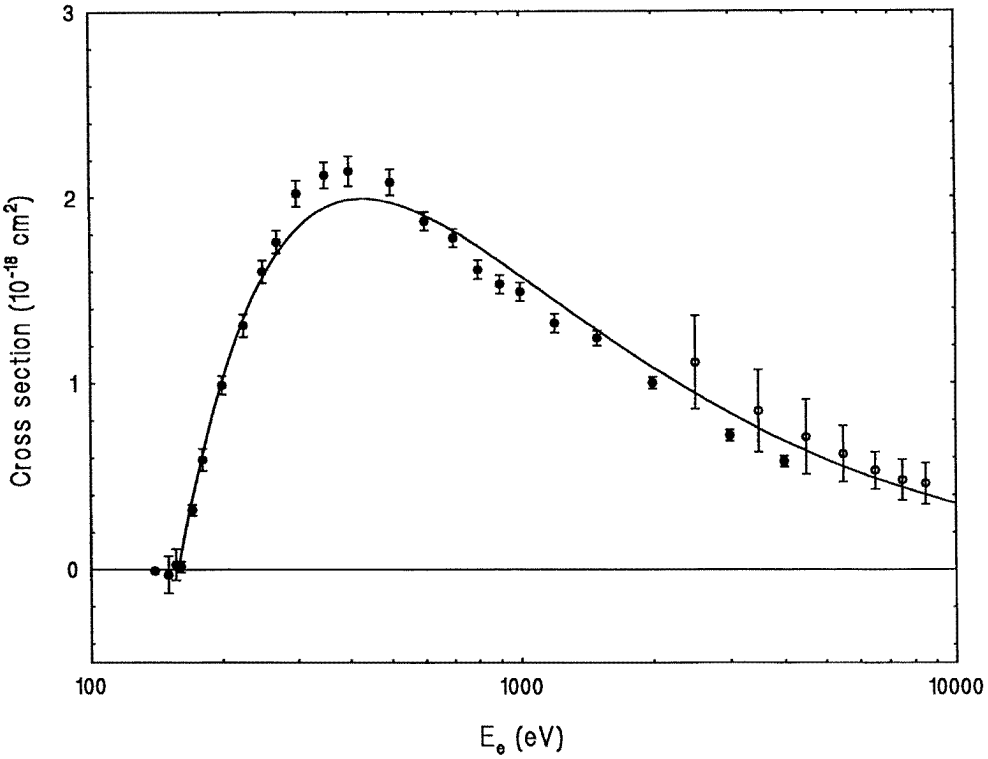

Figure 4. Absolute cross sections versus energy for electron-impact single ionization of Ne^{5+}. Full circles (●) are the present experimental results, error bars are of one standard deviation statistical uncertainty. The results of Donets and Ovsyannikov (1981) are also shown (○). The full curve is the semi-empirical Lotz formula.

threshold indicating the presence of an important metastable content which was found to be affected by large fluctuations depending on ion source conditions. The metastable population was estimated to reach some 50%.

Table 7. Total cross section for double ionization of Ne^{5+} by electron impact.

E_e (eV)	σ (10^{-20} cm^2)	$\Delta\sigma$ (10^{-20} cm^2)
350	−0.013	0.009
375	−0.014	0.005
390	0.001	0.006
400	0.016	0.007
450	0.041	0.012
500	0.09	0.02
550	0.15	0.02
600	0.22	0.02
650	0.21	0.02
700	0.20	0.02
750	0.21	0.02
800	0.26	0.02
900	0.25	0.02
1000	0.29	0.02
1050	0.32	0.01
1075	0.35	0.02
1100	0.47	0.03
1200	0.90	0.04
1300	1.18	0.04
1500	1.60	0.06
1700	1.88	0.06
2000	2.22	0.07
2200	2.38	0.07
2500	2.50	0.07
2700	2.55	0.07
3000	2.51	0.07
3200	2.62	0.07
3500	2.67	0.07
4000	2.62	0.08
5000	2.46	0.08

The single-ionization cross section is presented in figure 5(*b*) together with the experimental data of Donets and Ovzyannikov (1981) and with the recent theoretical results of Laghdas *et al* (1995).

In the low-energy region, only the direct ionization process plays a role. K–L excitation–autoionization is clearly found to contribute for some 7% of the total cross section at the corresponding threshold (888.3 eV). The role played by this indirect process in the beryllium isoelectronic sequence (Falk *et al* 1983) was found to be of the same order of magnitude for O^{4+}, but negligible for the lowest members of the sequence (B^+, C^{2+} and N^{3+}). K-shell ionization cannot contribute to single ionization, because the resulting Ne^{7+} ion is formed in the $1s2s^2\ ^2S$ state which is expected to be nearly totally autoionizing (99.3%) (Vainshtein and Safronova 1978), so that it will contribute to double ionization. This process will be discussed below.

Many theoretical calculations have been performed for this ion. Results were obtained by application of various Born approximations: Z-scaling (Sampson and Golden 1979), distorted-wave Born-exchange calculation (Younger 1981), Coulomb–Born exchange and distorted-wave Coulomb–Born exchange (Jakubowicz and Moores 1981). The method of Laghdas *et al* (1995) combines the distorted-wave Coulomb–Born approximation and the R-matrix theory. There is an overall good agreement between the results of these papers

Table 8. Total cross section for double ionization of Ne^{6+} by electron impact.

E_e (eV)	σ (10^{-20} cm^2)	$\Delta\sigma$ (10^{-20} cm^2)
441	0.06	0.05
501	−0.001	0.002
601	0.04	0.02
701	−0.008	0.008
726	0.002	0.008
736	0.016	0.010
751	0.028	0.012
801	0.040	0.013
901	0.031	0.014
951	0.029	0.016
1001	0.040	0.013
1071	0.032	0.011
1101	0.040	0.016
1151	0.24	0.02
1201	0.42	0.03
1301	0.81	0.06
1401	1.02	0.06
1501	1.34	0.06
1751	1.48	0.06
2001	1.99	0.09
2501	2.10	0.05
3001	2.21	0.09
3501	2.22	0.09
4001	2.28	0.09
4501	2.17	0.10
5001	2.15	0.07
5501	1.94	0.07
6001	2.18	0.09

as well as with the present results for direct ionization.

The enhancement of the cross section at the excitation–autoionization (EA) threshold is estimated to be $(5 \pm 2) \times 10^{-20}$ cm^2. Two of the above-mentioned calculations estimate the EA contribution via the $1s2s^22p$ ^1P and ^3P states: Sampson and Golden (1979) and Laghdas *et al* (1995) give this contribution a value of 2.1×10^{-19} cm^2 and 4.4×10^{-20} cm^2, respectively. The autoionization branching ratios are taken into account for both the ^1P and the ^3P state (92.1 and 99.8%, respectively, from Chen and Crasemannn (1987). The *R*-matrix calculation reproduces rather well the experimental results, both for direct ionization and for excitation–autoionization cross section. This type of calculation is presently the most appropriate ionization cross section estimate when indirect processes play a significant role.

4.4. Single ionization of Ne^{7+}

Much attention has been paid to the lithium isoelectronic sequence, due to the significant role of the K–L excitation–autoionization process, so that a lot of experimental and theoretical results are available for many members of the sequence. For Ne^{7+}, the present experimental data are in good agreement with the lower precision experimental results of Defrance *et al* (1990) (not shown in figure 6) as well as with the high-energy EBIS data of Donets and Ovzyiannikov (1981). There is also an overall good agreement between the different

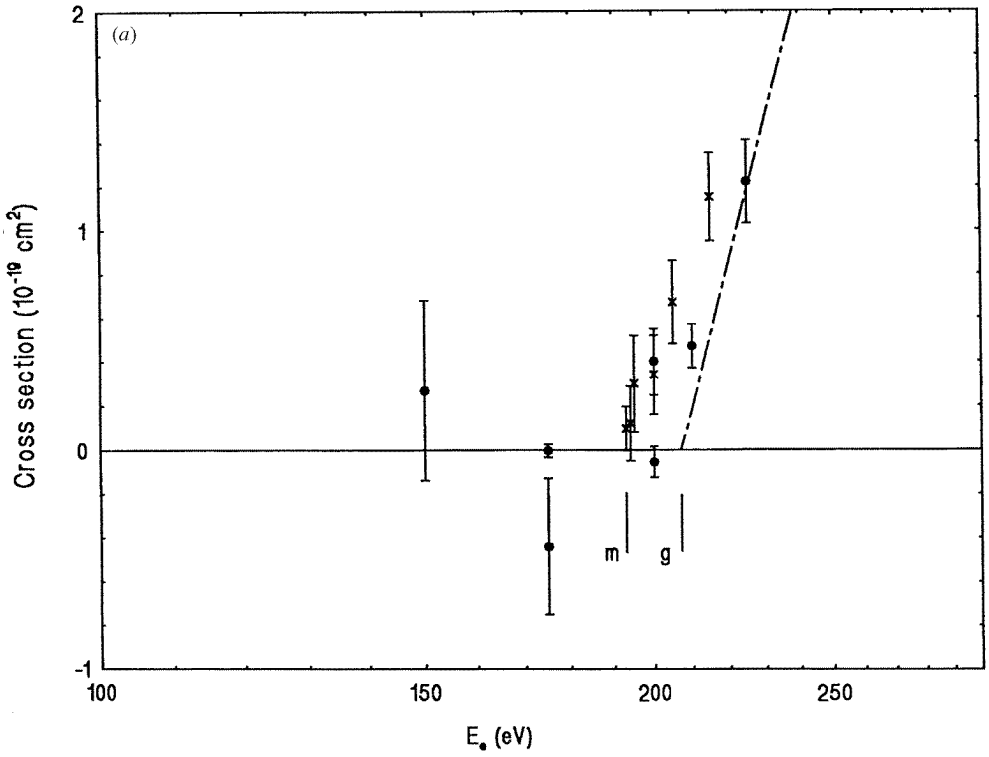

Figure 5. Absolute cross sections versus energy for electron-impact single ionization of Ne^{6+}. Symbols are (×) and (●) present experimental results with and without metastable states, respectively. Bars indicate the ionization thresholds for the ground state (g) and for the metastable state (m) and the excitation–autoionization threshold (E–A). Error bars are one standard deviation statistical uncertainty. The results of Donets and Ovsyannikov (1981) are also shown (○). The broken curve is the distorted-wave Coulomb–Born *R*-matrix calculation of Laghdas *et al* (1995).

theoretical results. The Coulomb–Born exchange (CBX) calculation of Jakubowicz and Moores (1981) includes direct ionization and excitation–autoionization. This calculation underestimates the direct ionization contribution below the K–L excitation threshold (891.1 eV), but the EA contribution is found to be in good agreement with the present data.

The K–L excitation–autoionization cross section can be estimated just above the excitation threshold if the direct process contribution can be precisely estimated in this energy region. The precision of present results allows the direct ionization cross section to be fitted by a standard formula from which the direct ionization cross section is extrapolated just above the excitation threshold. The extrapolated values are substracted from the experimental data, giving the estimation of the K–L excitation–autoionization cross section. The results of this procedure is also shown in figure 6. The excitation–autoionization cross section is estimated to be $4.3 \pm 0.5 \times 10^{-20}$ cm^2, a value which agrees with the theoretical result (4.1×10^{-20} cm^2) obtained by Goett and Sampson (1983). Taking into account the radiative decay of doubly excited states, this value reduces to 2.8×10^{-20} cm^2, the branching ratio for autoionization being estimated as 68% by Rachafi *et al* (1987). The comparison of these data indicates that the radiative decay of the autoionizing states concerned seems to be overestimated by the theory in the present situation.

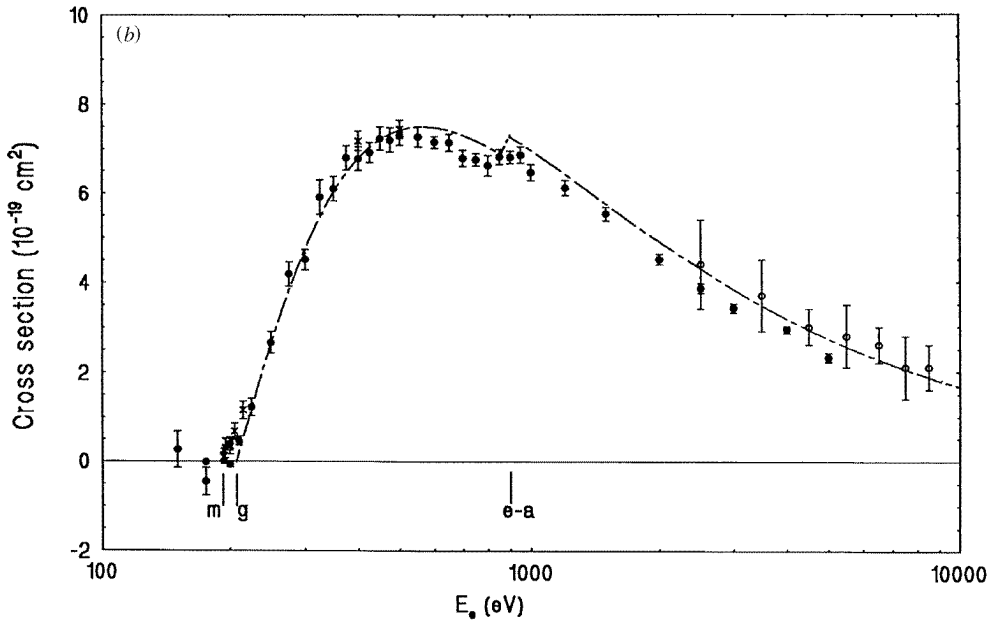

Figure 5. Continued.

4.5. Single ionization of Ne^{8+}

The electron-impact single-ionization cross section for Ne^{8+} is presented in figure 7. The inaccuracy of the experimental data is larger, due to the low-intensity ion current available. As mentioned above, the metastable states 1s2s (^{1}S and ^{3}S) contribution does not exceed the size of the error bars below the ground-state ionization threshold. The respective lifetimes of these states were estimated by Lin *et al* (1977) as 0.1 and 91 μs. The ion time of flight from the source to this region being 4.4 μs—the triplet state should still survive in the collision region. According to the size of the error bars and by applying the Lotz formula for the cross section estimation, the metastable fraction should be lower than 1%. This fraction was, however, found to be significant for lower charge ions belonging to the helium-like isoelectronic sequence (Rachafi *et al* 1989): 16% for C^{4+} and 4% for O^{6+}. The present data are in good agreement with the distorted-wave Coulomb–Born approximation (Younger 1980).

4.6. Double ionization of Ne^{5+} and Ne^{6+}

Double-ionization results are presented in figures 8 and 9 for Ne^{5+} and Ne^{6+}, respectively. It is evident that double ionization is dominated by the indirect K-shell IA process: the DDI contribution is an order of magnitude lower than the IA one for Ne^{5+} and is even nearly non-existent for Ne^{6+}. The IA process cross section can be roughly described by the Lotz formula, and by taking into account the above-mentioned autoionization branching ratios. This process was included in the *R*-matrix calculation for Ne^{6+} (Laghdas *et al* 1995) and the corresponding results are also shown in figure 9. The agreement of these predictions with each other and with the experimental results is satisfactory, in spite of the semi-empirical character of the Lotz formula.

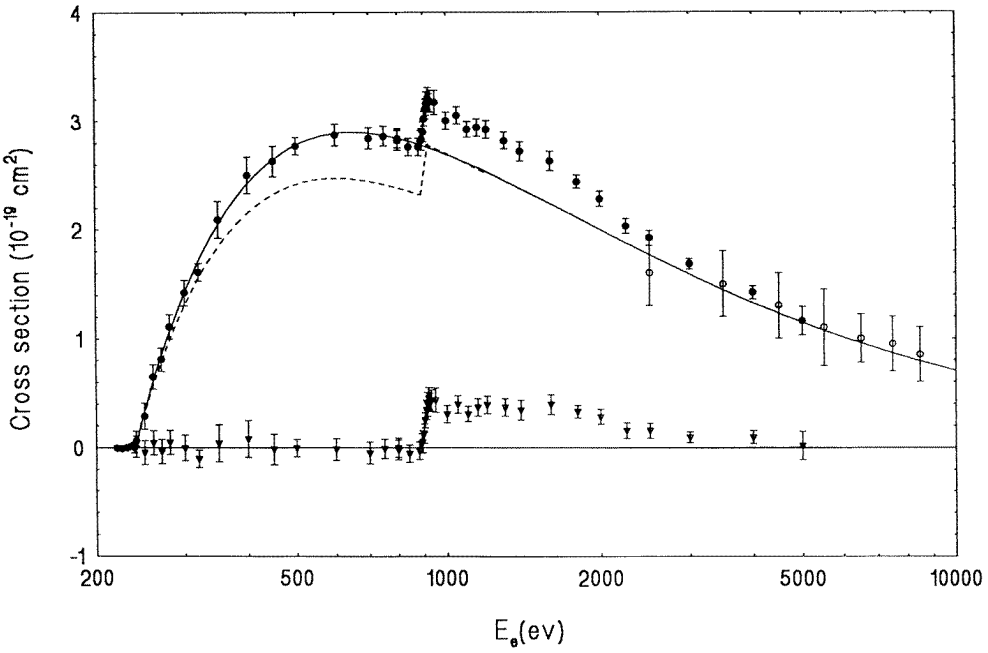

Figure 6. Absolute cross sections versus energy for electron-impact single ionization of Ne^{7+}. Full circles (●) are the present experimental results, the error bars are of one standard deviation statistical uncertainty. The results of Donets and Ovsyannikov (1981) are also shown (○). The full curve is the semi-empirical Lotz formula and the broken curve is the distorted-wave Coulomb–Born calculation of Jakubowicz and Moores (1981). Triangles show the excitation–autoionization contribution (see text).

For Ne^{5+}, the maximum DDI cross section is 2.6×10^{-21} cm^2, that is, only about 10% of the total cross section. Ne^{5+} belongs to the boron isoelectronic sequence. The lowest charge state ion of this sequence is C^+, for which double-ionization cross section is known (Zambra *et al* 1994). The results show that DDI and IA play a roughly equivalent role in C^{3+} production, which is totally different for Ne^{7+} production in the present case. But, the classical scaling law predicts that the ionization cross section varies inversely with the square of the ionization potential (I_2). The present result suggests that the DDI cross section (σ_D) reduces more rapidly than predicted by the classical scaling law along the isoelectronic sequence:

$$\sigma_D = \frac{A}{I_2^2}\,. \tag{4}$$

A is obtained from the experimental data below the IA threshold around the maximum of the DDI cross section, both for C^+ and for Ne^{5+}. The ratio between the respective values is found to be 0.32, that is, well below 1. This result demonstrates that A reduces with increasing ion charge. New data are needed for other members of the isoelectronic sequence in order to determine more precisely the charge dependence of the DDI cross section.

For Ne^{6+}, the DDI cross section is too small to be clearly identified. The detail of the cross section below the K-shell ionization threshold shows a weak but significant signal (the maximum is 4×10^{-22} cm^2), presenting an apparent threshold at 730 eV. The lowest DDI threshold is at 446.4 eV and no reaction was found to have such a particular ionization

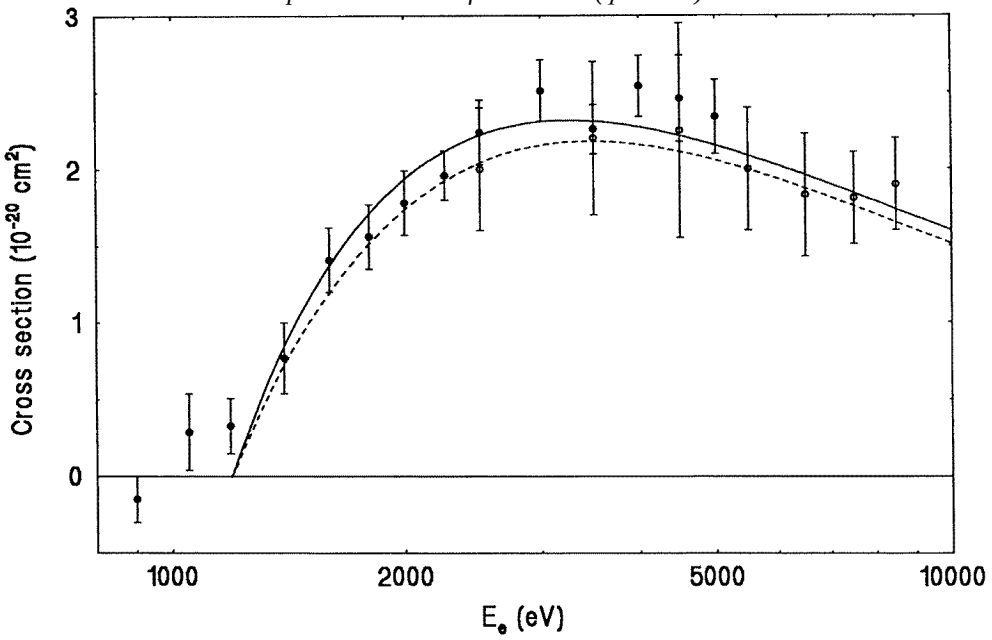

Figure 7. Absolute cross sections versus energy for electron-impact single ionization of Ne^{8+}. Full circles (●) are the present experimental results, the error bars are of one standard deviation statistical uncertainty. The results of Donets and Ovsyannikov (1981) are also shown (○). The full curve is the semi-empirical Lotz formula and the broken curve is the distorted-wave Coulomb–Born calculation of Younger (1980).

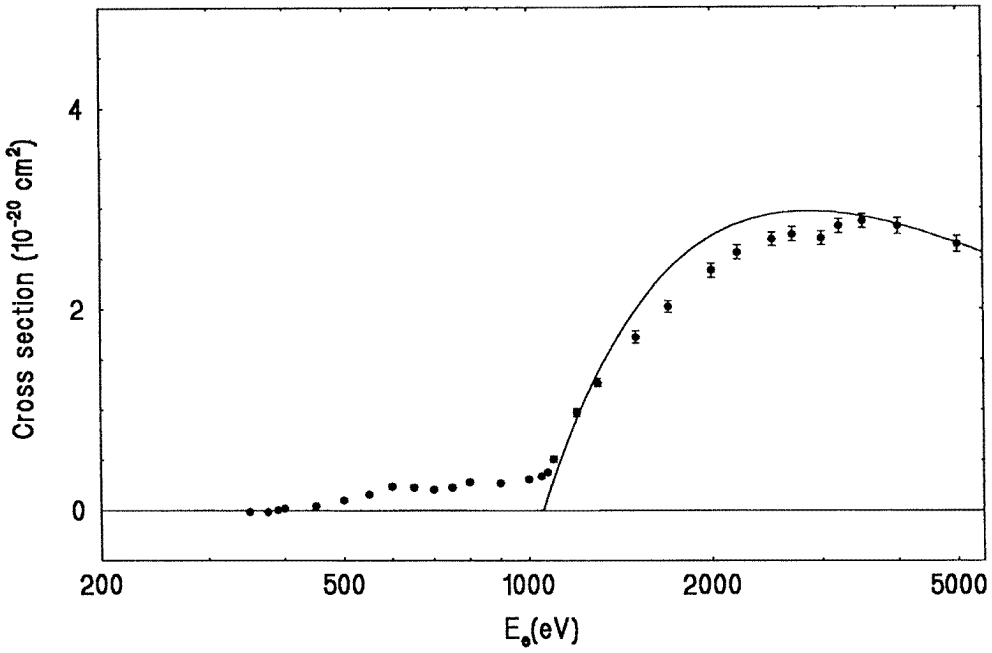

Figure 8. Absolute cross sections versus energy for electron-impact double ionization of Ne^{5+}. Full circles (●) are the present experimental results, the error bars are of one standard deviation statistical uncertainty. The full curve is the semi-empirical Lotz formula for K-shell ionization, only.

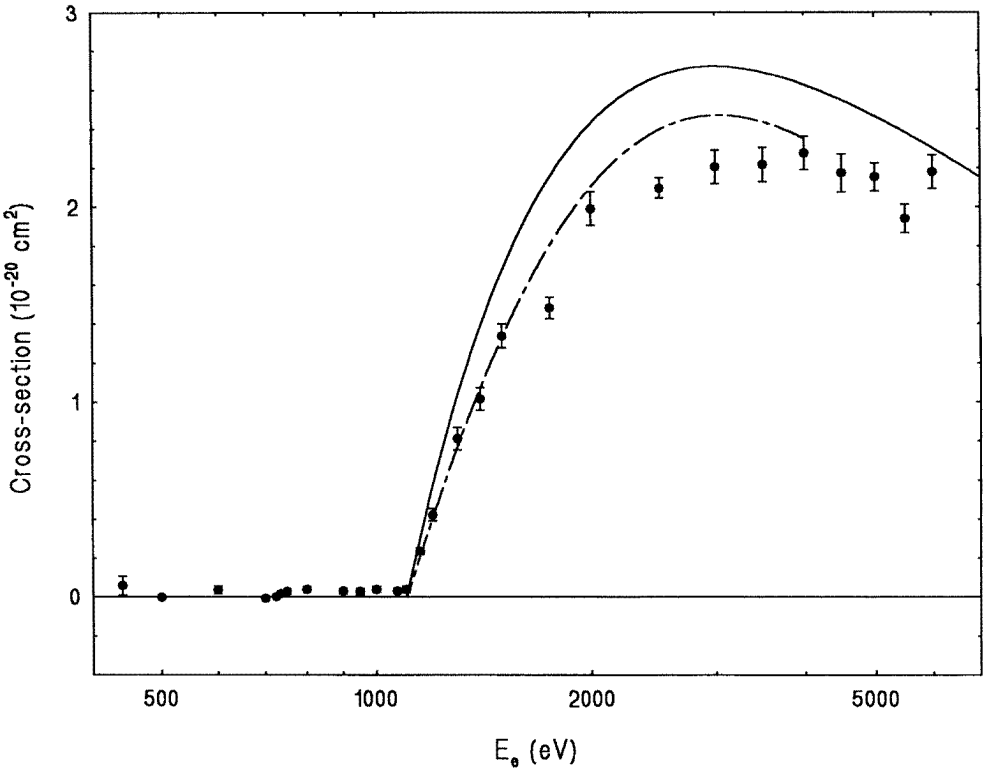

Figure 9. Absolute cross sections versus energy for electron-impact double ionization of Ne^{6+}. Full circles (●) are the present experimental results, the error bars are of one standard deviation statistical uncertainty. The full curve is the semi-empirical Lotz formula for K-shell ionization, only. The broken curve is the *R*-matrix calculation of Laghdas *et al* (1995).

threshold, or from the ground state, or from the metastable state. In any case, DDI is almost non-existent for Ne^{6+}. No argument or scaling procedure can be put forward to predict such a result.

5. Summary

Absolute cross sections are reported for single ionization of multiply charged Ne^{q+} ($q = 4$–8) ions and for double ionization of Ne^{5+} and Ne^{6+}. The role of ions formed in metastable states is observed for Ne^{4+} and for Ne^{6+} but not for Ne^{8+}. For single ionization, the direct ionization cross section is found in good agreement with the predictions of the semi-empirical Lotz formula ($q = 4$, 5) and with results of the Coulomb–Born approximation calculations when available ($q = 6$–8). K–L excitation–autoionization is seen to play a role for Ne^{6+} and for Ne^{7+}. In the latter case, the corresponding estimated cross section is in good agreement with the theoretical results without inclusion of radiative decay of doubly excited states.

Double ionization of Ne^{5+} and Ne^{6+} is dominated by K-shell ionization followed by autoionization. The comparison of the results for two members of the boron isoelectronic sequence (C^+ and Ne^{5+}) demonstrates that the classical scaling law is invalid for direct double ionization.

Acknowledgments

This work was supported by the European Commission (contract SC1-0470). The authors acknowledge the members of the Centre de Recherche du Cyclotron for technical support.

References

Bashkin S and Stoner J 1975 *Atomic Energy Levels and Grotrian Diagrams* vol II (Amsterdam: North-Holland) (1978 addenda)
Bliman S, Bonnefoy M, Bonnet J J, Dousson S, Fleury A, Hitz D and Jacquot B 1983 *Phys. Scr.* T **3** 63
Chen M H and Crasemann B 1987 *At. Data Nucl. Data Tables* **37** 419
Cheng K T, Kim Y K and Desclaux J P 1979 *At. Data Nucl. Data Tables* **24** 111
Clementi E and Roetti C 1974 *At. Data Nucl. Data Tables* **14** 177
Defrance P, Brouillard F, Claeys W and Van Wassenhove G 1981 *J. Phys. B: At. Mol. Phys.* **14** 103
Defrance P, Chantrenne S, Rachafi S, Belic D S, Jureta J, Gregory D C and Brouillard F 1990 *J. Phys. B: At. Mol. Opt. Phys.* **23** 2333
Defrance P, Duponchelle M and Moores D L 1995 *Atomic and Molecular Processes in Fusion Edge Plasmas* ed R K Janev (New York: Plenum) p 153
Donets E D and Ovzyannikov V P 1981 *Sov. Phys.–JETP* **53** 466
Duponchelle M, Zhang H, Oualim E M, Bélenger C and Defrance P 1995 *Nucl. Instrum. Methods.* A **364** 159
Falk R A, Stefani G, Camilloni R, Dunn G H, Phaneuf R A, Gregory D C and Crandall D H 1983 *Phys. Rev.* A **28** 91
Goett S J and Sampson D H 1983 *At. Data Nucl. Data Tables* **29** 535
Gregory D C, Crandall D H, Phaneuf R A, Howald A M, Dunn G H, Falk R A, Mueller D W and Morgan T J 1985 Oak Ridge National Laboratory *Report* ORNL/TM-9501
Gregory D C, Dittner P F and Crandall D H 1983 *Phys. Rev.* A **27** 724
Jakubowicz H and Moores D L 1981 *J. Phys. B: At. Mol. Phys.* **14** 3733
Janev R K 1993 Summary report of the IAEA technical committee meeting on atomic and molecular data for fusion reactor technology *Report INDC(NDS-277)* (Vienna: IAEA)
Laghdas K 1995 *Thesis* Université libre de Bruxelles
Laghdas K, Reid R H G, Joachain C J and Burke P G 1995 *Proc. 19th Int. Conf. on Physics of Electronic and Atomic Collisions (Whistler)* ed J B A Mitchell, J W Mc Conkey and C E Brion p 563
Lennon M A, Bell K L, Gilbody H B, Hughes J G, Kingston A E, Murray M J and Smith F J 1988 *J. Chem. Ref. Data* **17** 1285
Lin C D, Johnson W R and Dalgarno A 1977 *Phys. Rev.* A **15** 158
Lotz W 1968 *Z. Phys.* **216** 241
Man K F, Smith A C H and Harrison M F A 1987 *J. Phys. B: At. Mol. Phys.* **20** 5865
Matsumuto A, Danjo A, Ohtani S, Suzuki H, Tawara H, Takayanagi T, Wakiya K, Yamada I, Yoshino M and Hirayama T 1990 *J. Phys. Soc. Japan* **59** 902
Rachafi S, Defrance P and Brouillard F 1987 *J. Phys. B: At. Mol. Phys.* **20** L665
Rachafi S, Zambra M, Zhang Hui, Duponchelle M, Jureta J and Defrance P 1989 *Phys. Scr.* **28** 12
Sampson D H and Golden L B 1979 *J. Phys. B: At. Mol. Phys.* **12** L785
Schumann S, Groeneveld K O, Sevier K D and Fricke B 1977 *Phys. Lett.* **60A** 289
Vainshtein L A and Safronova V I 1978 *At. Data Nucl. Data Tables* **21** 49
Younger S M 1980 *Phys. Rev.* A **22** 1425
——1981 *Phys. Rev.* A **24** 1278
Zambra M, Belic D, Defrance P and Yu D J 1994 *J. Phys. B: At. Mol. Opt. Phys.* **27** 2383